Edinburgh Research Explorer

Three-Dimensional Architecture and Surface Functionality of Coccolith Base Plates

Three-Dimensional Architecture and Surface Functionality of Coccolith Base Plates

B. Marzec,[1,†] J. M. Walker,[1,‡] M. Panagopoulou,[2] Y. Jhons,[1] D. Clare,[3] A. Wheeler,[4] M. P. Shaver[5] and F. Nudelman[1]*

[1] School of Chemistry, University of Edinburgh, King's Buildings, Edinburgh, EH9 3FJ, United Kingdom.

[2] MRC Centre for Inflammation Research, University of Edinburgh, 47 Little France Crescent, Edinburgh, EH16 4TJ, United Kingdom.

[3] Electron Bio-Imaging Centre, Diamond Light Source Ltd., Harwell Science & Innovation Campus, Didcot, OX11 0DE, United Kingdom.

[4] MRC Human Genetics Unit, Institute of Genetics and Molecular Medicine, University of Edinburgh, Crewe Road, Edinburgh, EH4 2XU, United Kingdom.

[5] School of Materials, The University of Manchester, Oxford Road, Manchester, M13 9PL, United Kingdom

Present addresses:

†   JEOL (UK) Ltd., Silver Court, Welwyn Garden City, AL7 1LT, United Kingdom.

‡   McCormick School of Engineering, Northwestern University, 2220 Campus Drive, Cook Hall 2036, Evanston, IL 60208, United States of America.

*Corresponding author: fabio.nudelman@ed.ac.uk

Abstract

Coccolithophores are marine phytoplankton that are among the most prolific calcifiers widespread in Earth's oceans, playing a crucial role in the carbon cycle and in the transport of organic matter to the deep sea. These organisms produce highly complex mineralized scales that are composed of hierarchical assemblies of nano-crystals of calcium carbonate in the form of calcite. Coccolith formation *in vivo* occurs within compartmentalized mineralisation vesicles derived from the Golgi body, which contain coccolith-associated polysaccharides ('CAPs') providing polymorph selection and mediating crystal growth kinetics, and oval organic mineralisation templates, also known as base plates, which promote heterogenous nucleation and further mechanical interlocking of calcite single crystals. Although the function of coccolith base plates in controlling crystal nucleation have been widely studied, their 3D spatial organization and the chemical functional groups present on the crystal nucleation sites, which are two crucial features impacting biomineralization, remain unsolved. Utilising cryo-electron tomography we show that base plates derived from an exemplary coccolithophore *Pleurochrysis carterae* (Pcar) in their native hydrated state have a complex 3-layered structure. We further demonstrate, for the first time, the edge and rim of the base plate – where the crystals nucleate - are rich in primary amine functionalities that provide binding targets for negatively charged complexes composed of synthetic macromolecules and Ca^{2+} ions. Our results indicate that electrostatic interactions between the negatively charged biogenic CAPs and the positively charged rim of the base plate are sufficient to mediate the transport of Ca^{2+} cations to the mineralization sites.

1. Introduction

In nature, organisms from all kingdoms are known to produce a wide range of mineralised tissues that fulfil a variety of functions and play a crucial role in survival, including navigation, mechanical support and protection (Lowenstam and Weiner, 1989). Among the many mineralising organisms, coccolithophores are one of the most interesting. They are marine phytoplankton that display a remarkable ability to orchestrate the multi-level assembly of mineral building blocks into a higher order structure, producing polycrystalline scales made of $CaCO_3$ in the form of calcite called coccoliths (Young et al., 1992). The precise genetic control these organisms exert over the nucleation, morphology, orientation and organisation of the crystals is further highlighted by the fact that coccolith shape, structure, size and arrangement of the crystals is genus-specific (Manton and Leedale, 1969; Outka and Williams, 1971). Understanding how such distinctive and sophisticated mineral patterns and morphologies are generated is a long-standing question that still needs to be solved.

Coccolith synthesis occurs inside a specialised intracellular compartment, the coccolith vesicle (van der Wal et al., 1983; Young et al., 1999). It starts with the nucleation of calcite crystals on the rim of an oval-shaped organic scaffold termed base plate, forming the protococcolith ring (Marsh, 1999; Young et al., 1992). At this stage, the crystals have alternating crystallographic orientations, and as they grow selectively along specific directions they mechanically interlock, leading to the formation of the mature coccolith. Coccolith-associated polysaccharides (CAPs) have been shown to play a crucial role in the mineralization process by being involved in the transport of Ca^{2+} ions (Gal et al., 2016; Marsh, 1994; Marsh, 1999; Taylor et al., 2017), regulating crystal morphology (Henriksen et al., 2004; Kayano et al., 2011) and determining polymorph type (Walker et al., 2019).

Given the central role of the base plates as scaffolds for mineral formation, there are two key factors that need to be determined in order to elucidate its function in mediating crystal nucleation: its 3D structure and architecture, and its surface chemistry. Early transmission electron microscopy (TEM) measurements of dehydrated base plates from *Pleurochrysis carterae* prepared using gold-shadowing techniques showed that these scaffolds display two morphologically different sides: the "bottom" side, ornamented with ridges radiating from the center, and the "top" side, devoid of any patterning, with the latter being the surface that supports crystal nucleation (Pienaar, 1969). Subsequent TEM analysis on dehydrated and negatively stained base plates revealed that the top side is not devoid of patterning, but in fact displays planar networks of concentric and radial ribbon-shaped fibrils that were 6 − 7 nm in diameter (Franke and Brown, 1971). A similar surface topography was also observed more recently using atomic force microscopy (AFM) on dry specimens (Gal et al., 2016). Although these studies were important in revealing the surface architecture of the base plates, they were limited in that the sample preparations used required dehydration, which is known to cause artefacts such as shrinkage of the biological material. Furthermore, TEM images are 2D projections of 3D objects, while AFM is a surface technique. To date, no further work to characterize the structure of the base plates has been done, and our current understanding of the structure and architecture of this scaffold is still incomplete, as it relies on extrapolating a 3D model from 2D TEM projections and from surface measurements, both taken from dehydrated specimens.

Little is known about the surface chemistry of the base plates. It has been proposed that a folded ribbon-like template containing a chequerboard-like pattern of nucleation sites is present on the rim of the base plates and is responsible for the alternate crystallographic orientation of the crystals in the coccolith (Marsh, 1999). The chemical functional groups that constitute the nucleation sites on this template are still unknown. It was recently shown that acidic polysaccharides from *P. carterae* recognize the sites on the rim of the base plate that support calcite nucleation and directs Ca^{2+} ions to those areas (Gal et al., 2016). Based on that, it was proposed that this binding was mediated by specific macromolecular recognition between the polysaccharides and the rim of the base plates. It was further suggested that proteins located close to the rim act as a binding target for CAP/Ca^{2+} complexes (Sakurada et al., 2018).

Looking at these advances, a complex picture of coccolith formation emerges. Firstly, Ca^{2+} ions, which are stored in a calcium and phosphate-rich compartment (Gal et al., 2018; Gal et al., 2017b; Sviben et al.,

2016), bind to CAPs and are transported *via* a yet undiscovered mechanism to a mineralization vesicle pre-equipped with a base plate (Wilbur and Watabe, 1963). Acidic CAPs recognize proteins present on the base plate rim and deliver Ca^{2+} ions to this specific area, leading to calcite nucleation. These observations suggest that the rim of the base plates, where crystal nucleation takes place, must be chemically different from the central area, so as to ensure the specific binding of the polysaccharides-Ca^{2+} complexes, followed by crystal nucleation. Information on the nature of the nucleation sites, in particular which chemical functional groups are present and how they interact with the mineral is still missing.

Here, we used cryoTEM, specimen staining, and cryo-electron tompgraphy (cryoET) to characterize the three-dimensional structure and architecture of coccolith base plates in their native, hydrated state, minimizing artefacts caused by sample preparation. Using a combination of cryoTEM, cryoET and super-resolution fluorescence microscopy, we provide evidence suggesting that the rim of the base plates – the site that supports crystal nucleation – is functionalized with positively charged primary amines. We propose that these functional groups mediate the binding of negatively charged CAP complexes/Ca^{2+} ions through electrostatic interactions, and promote crystal nucleation.

2. Materials and Methods

All chemicals were purchased in the highest available purity grade and – unless stated otherwise – used as received, without any further purification.

Algae cultures: Starting cultures of cells belonging to the species *Pleurochrysis carterae*, strain 961/1, were purchased from the Culture Collection of Algae and Protozoa, SAMS Ltd., Scottish Marine Institute, Dunbeg, Oban, Argyll, PA37 1QA, UK. The cells were subcultured using the Guillard's F/2 medium, whereby the growth mixtures were composed of 29 mL of seawater (collected from North Atlantic and provided by SAMS Ltd., filtered), 600 μL of the Guillard's (F/2) marine water enrichment solution (50x concentrated, Sigma Aldrich, cat. no. G9903) and 300 μL of the antibiotics solution (penicillin (5000 u·mL^{-1}) – streptomycin (5 mg·mL^{-1}) – neomycin (10 mg·mL^{-1}) solution stabilized, Sigma Aldrich, cat. no. P4083). Cultures were kept in an incubator (Panasonic MLR-352 Versatile Environmental Test Chamber), which maintained the temperature of 15 °C and provided a photon flux density of 200 μmol·m^{-2}·s^{-1} following the 12 h day / 12 h night cycle. Following the exponential growth phase, the amount of the cells in the growth medium stabilized at *ca.* $3.5 \cdot 10^6$ cells·mL^{-1} after 9 days of incubation.

Cryo-TEM sample preparation – base plates: 100 μL of Pcar cultures whose growth achieved the plateau stage were transferred to a 1 mL centrifuge tube and mixed with 100 μL of 20 nm large gold nanoparticles solution stabilised in a citrate buffer (Sigma Aldrich, cat. no. 741965). The obtained mixture was shaken vigorously for 1 minute. 3 μL of the mixture were then deposited on a TEM grid (Quantifoil GmbH, 2 μm hole, 2 μm gap, cat. no. R2/2) located in a Vitrobot (FEI, Mark IV). 2 μL of 50 % aqueous solution of acetic acid were added directly to the grid in order to dissolve the calcite crystals and liberate the base plates. After 30 seconds the grid was blotted (FEI Vitrobot Mk IV, blot time: 1.5 s, blot force: 4) and plunge-frozen in liquid ethane to vitrify the organic material. Following freezing, the TEM grids were stored under liquid nitrogen for no longer than 7 days.

Cryo-TEM sample preparation – stained base plates: 50 mL of Pcar cultures were centrifuged and the obtained white solid, consisting of the cells, was re-dispersed in 10 % (v/v) aqueous solution of Triton X-100 (Sigma Aldrich, cat. no. 93443). After 12 hours, this solution was centrifuged, which led to the deposition of a white precipitate at the bottom of the centrifuge tube. SEM analysis of that material confirmed that it was composed of Pcar coccoliths. The obtained solid was re-dispersed in seawater and centrifuged again in order to remove all residual Triton X-100 and other impurities of cellular origin. Following purification, the coccolith sample was dispersed in a 3 % (v/v) aqueous solution of acetic acid, which dissolved calcite crystals and liberated the base plates. The obtained base plates suspension (25 mL) was then dialyzed for 72 hours against deionized water (5 L) using a membrane with a 1000 Da cut-off point in order to remove the excess of acetic acid and acetic acid-Ca^{2+} complexes. After 72 hours the dialysis was carried out again using fresh deionized water. The base plates was centrifuged and the excess of water was disposed, whereby the final volume of the suspension was 10 mL. Sodium azide (0.02 %) was

added to the sample to prevent any bacterial growth. The suspension was stored at 4 °C and used when required as the stock solution.

Staining with sodium phosphotungstate, poly(acrylic acid) / Ca^{2+} mixture and poly(allylamine hydrochloride) / CO_3^{2-} mixture was carried out directly on TEM grids (Quantifoil, GmbH, 2 µm hole, 2 µm gap, cat. no. R2/2). In a typical procedure, 2 µL of the base plate suspension were mixed with 2 µL of the citrate buffer stabilized suspension of 10 nm large gold nanoparticles (Sigma Aldrich, cat. no. 741957), and with 2 µL of the stain (see below). The concentrations of the stains were as follows: sodium phosphotungstate – 3% (w/v); PAA/Ca^{2+} - 0.25% (w/v) PAA (Mw 8000 g/mol) in 10 µM $CaCl_2$; PAH/CO_3^{2-} - 0.25% (w/v) PAH (Mw 17500 g/mol) in 10 mM Na_2CO_3. The base plates were allowed to react with the stains for 30 seconds. After that time the TEM grids were blotted and vitrified.

Cryo-electron tomography: Imaging was carried out using either the FEI Tecnai F20 microscope operating at 200 keV and equipped with a Tietz 8k x 8k camera (stained base plates), or the FEI Titan Krios microscope operating at 300 keV and equipped with a Gatan K2 Summit 4k x 4k camera and a Volta phase plate (unstained base plate at high magnification). Tilt series were recorded with the SerialEM software package in the -60° to 60° range using 1.5° step, whereby the total electron-dose did not exceed 46 $e^-\cdot A^-2$. Tomograms were reconstructed from the recorded tilt series using the IMOD package, whereby the gold nanoparticles were used as fiducial markers.(Kremer et al., 1996) Tomogram filtering and final segmentation were carried out using the FEI Avizo software suite, whereby the intensity threshold was selected arbitrary to provide the optimal signal/nose ratio.

Super Resolution Radial Fluctuations Microscopy (SRRF): Similarly to cryoTEM staining, base plates for SRRF analysis were derived from mature Pcar coccoliths by treating them with 3% acetic acid solution and purifying the obtained suspension by dialysis against deionized water (cut-off point 1 kDa) for 72 hours. The base plates were then centrifuged, suspended in 1 ml of 10 mM carbonate buffer containing 0.02 % of sodium azide whose pH was adjusted to 7.4 using sodium hydroxide. Reaction with the succinimidyl ester (NHS ester) of Alexa 488 fluorophore (ThermoFisher Scientific, cat. no. A20000) was done by adding 100 µl of a DMSO solution containing 10 mg/ml of the dye. The reaction was carried out at room temperature for 2 hours, whereby the sample was constantly shaken with a shaker (45 rpm). Following that time, the base plates were embedded in the ProLong Diamond Antifade Mountant resin (ThermoFisher Scientific, cat. no. P36970), and imaged using Nikon N-SIM microscope. The recorded SRRF data were processed using ImageJ equipped with the Nano-SRRF plugin.

3D-Structured Illumination Microscopy (SIM): Samples used for SIM imaging were prepared following the same protocol as the one applied for SRRF and described above. Briefly - Pcar base plates were obtained by treating mature coccoliths with 3% acetic acid and dialyzing the obtained suspension against deionized water for 72 hours using a membrane with a 1 kDa cut-off point. After that time, the base plates were centrifuged and re-suspended in 1 mL of deionized water containing 0.02% of sodium azide (acting as a preservant). 100 µL of that suspension was then mixed with 100 µL of 0.25% (v/v) fluorophore solution in deionised water or in 10 mM Na_2CO_3, and the obtained mixture was shaken for 12 hours. After that time, 10 µL of the suspension was deposited on a low-background glass slide, fixed with a glass cover slip, and imaged using Nikon N-SIM microscope. Where required, the samples were diluted either 10 times or 100 times prior to imaging in order to provide low background and maximise the signal to noise ratio. The SIM data were reconstructed using the NIS-Elements software equipped with the NIS-A N-SIM Analysis module. Fluorophores used in the study included the poly(allylamine hydrochloride) containing *ca.* 2% units substituted with fluorescein ('PAH-FL'), and poly(acrylic acid) containing *ca.* 2% units substituted with Rhodamine 123 ('PAA-R'). These fluorescent polymers were prepared according to the procedures described below.

Rhodamine 123, 1-Ethyl-3-(3-dimethylaminopropyl)carbodiimide (EDC) and N-hydroxysulfosuccinimide sodium salt (HSSS) were purchased from Sigma Aldrich. Dimethylformamide (DMF) was purchased from Fischer Scientific and the distilled water was ultragrade pure from a satorius water purification system. Poly(acrylic acid) (50 000 g·mol^{-1}) 25 % solution in water was purchased from Polysciences Inc. The Spectra/Por 1 dialysis membrane was purchased from VWR, with a MWCO of 6 – 8 kD. The poly(acrylic

acid) was dialyzed against water for 2 days followed being freeze dried to purify the reagent. All other reagents were used as received.

General considerations: Samples were freeze dried using a Lablyo mini freeze dryer

Synthesis of poly(acrylic acid-*co*-(rhodamine 123)) ('PAA-R'): The synthesis is modified from literature.(Laguecir et al., 2006) EDC (2 mg, $1.31 \cdot 10^{-2}$ mmol) and NHS (2.84 mg, $1.31 \cdot 10^{-2}$ mmol) were dissolved in 0.2 mL of water and added to a solution of PAA (0.328 g, $6.6 \cdot 10^{-3}$ mmol) in 6 mL of water. Afterwards rhodamine 123 (2 per PAA chain, 5.00 mg, $1.31 \cdot 10^{-2}$ mmol) in 3 mL of DMF was added to the solution. The mixture was left stirring for 24 hours at room temperature. After 24 hrs stirring the mixture was placed into a dialysis membrane and dialyzed against water for 2 days then freeze dried, yielding an orange powder (0.261 g, 80 %).

Synthesis of poly(allylamine hydrochloride-*co*-(fluorescein)) ('PAH-FL'): Fluorescein-labelled poly(allylamine hydrochloride) was synthesized from 15 000 g·mol^{-1} PAH (Sigma-Aldrich, cat. no. 283215) and fluorescein isothiocyanate (Sigma-Aldrich, cat. no. F4274) followed by recrystallization and lyophilisation under vacuum, according to previously published procedures.(Begum et al., 2010)

3. Results:

3.1 Three-dimensional structure of the base plate

Base plates from *Pleurochrysis carterae* (Pcar) were isolated by treating mature coccoliths (Fig. 1A-B) with 3% acetic acid and dialyzing the obtained suspension against seawater. The purified base plates were then concentrated by centrifugation, mixed with a suspension of 10 nm gold nanoparticles acting as fiducial markers, deposited on TEM grids, vitrified in liquid ethane and imaged using cryoTEM. The obtained base plates were *ca.* 900 nm x 1.3 µm large and their ellipsoidal shape was comparable with that of mature Pcar coccoliths (Fig. 1C). As shown in Fig. 1D, high magnification images confirmed that the base plates display a fibrous structure that appears to include both radial and concentric fibers. These features, however, are absent from a 45 nm-wide region corresponding to the rim of the base plates. Finally, the base plates are delineated by a 10 nm-thick border (black arrow). Overall this structure, visualized in 2D, is in agreement with previous literature reports (Pienaar, 1969; Franke and Brown, 1971). Importantly, since our images were taken from base plates in their native, hydrated state, we can ensure that all the structural features observed are an integral part of the architecture of the base plate, rather than artefacts from drying or shadow-casting.

Since the cryoTEM images are 2D projections of a 3D object, all the features observed, including the radial and concentric fibrous networks, are superimposed. Thus, it is not possible to discern how they are organized within the base plate - whether they are on the same plane or form different layers, and what the architecture of the base plate in 3D is. To solve this, we performed cryoET on the base plate depicted in fig. 1D, whereby the sample was tilted between -60 ° and +60° and images were recorded at each tilt angle. The images were then used to reconstruct the 3D object. This technique revealed that the base plates consisted of three distinct layers, surrounded by a *ca.* 20 nm high rim (Fig 2 and Fig. S1): a bottom side, which was composed of *ca.* 3 nm thick fibers built into lamellar layers forming V-shaped connections between different regions (Figs. 2A and 2D, in green), similar to previous reports. These fibers extended from the center of the base plate all the way to the rim, even protruding from the external border. The second layer consists of fibers in a circular arrangement disposed on top of the radial ones at the bottom layer (Figs. 2B and 2D, in yellow). Importantly, the 45 nm-wide rim of the base plate did not display any structural features, similar to the 2D image (Fig. 1D) and confirming previous dry AFM observations (Gal et al., 2016). The third and top layer of the base plate consisted of a fine, disordered meshwork of fibers, each *ca*. 2-3 nm in diameter, covering most of the surface of the base plate (Figs. 2C and 2D, in red). The rim of the base plate, on the other hand, had a different structure. It consisted of a 100 nm-wide region extending from the border of the base plate and displaying a globular-like structure (Figs. 2C and 2D, in red). It did not contain any of the disordered meshwork of fibers observed on the remaining surface of

the base plate. This third structural level of the base plate are reported here for the first time. Taken together, using cryoET to characterize base plates in their native, hydrated state, we show how the different structural elements that compose this scaffold are organized in 3D, forming a substrate that supports crystal nucleation and growth in coccolithophores. We show that this scaffold contains 3 layers displaying different structures, which suggests that they have different compositions. Importantly, the rim of the base plate, which is the site where the crystals nucleate, is structurally different from the central part of the base plate in the middle and top layers, exhibiting a globular-like texture instead of a network of fibers.

3.2 Chemical staining of the base plate

Considering that the rim of the base plate is the site where calcite crystals nucleate, its chemical composition is likely to differ when compared with the base plate central region. In particular, this region must contain chemical functional groups that direct the binding of Ca^{2+}-polysaccharide complexes and promote crystal nucleation. Therefore, our next step was to use cryoTEM, cryoET and super-resolution radial fluctuations ('SRRF') microscopy to probe the chemical functionality of the rim of the base plate. These experiments were done on decalcified base plates, exposing the sites in the rim where crystal nucleation took place. This approach follows similar chemical mapping of the organic matrix of the nacreous layer of mollusks shells (Crenshaw and Ristedt, 1976; Nudelman et al., 2006).

In the first step to identify the chemical functional groups present on the rim of the base plates, we combined positive staining with sodium phosphotungstate with cryoTEM. The aim of this experiment was to probe whether the staining agent would bind selectively to any region of the base plates due to charge interactions. As shown in Fig. 3, sodium phosphotungstate, which offers specificity towards positively charged species (Jackson et al., 1998), interacted preferentially with the base plate edge and rim (Fig. 3A-B), suggesting that these areas are positively charged (Ackermann, 2009). Our observations are further substantiated by the work of M. Marsh *et* al., (Protoplasma 1999) where lead citrate had been used as a staining agent. The observed staining pattern had resembled the one presented here for samples stained with sodium phosphotungstate. It indicates that molecules equipped with multiple functional groups and capable of acting as polydentate chelators, such as citrate anions, can facilitate the attachment of metal ions to the base plate rim by bridging between the positively charged surface and the metal ions (Chu et al., 2011; Drzewiecka-Antonik et al., 2017). These observations point to the non-specific nature of the interactions between the staining agents and the rim of the base plate, whereby metal ions characterized with substantially different chemical properties were confirmed to bind to the base plate rim either directly or in the presence of a suitable anion.

To investigate further the surface charge of the rim, we probed whether polymers without secondary structure, equipped with either positively or negatively charged functional groups could bind to the base plates. As shown in Fig. 4A, a negatively charged mixture of poly(acrylic acid) ('PAA') with 10 µM Ca^{2+} (ζ-potential of -9 ± 0.6 mV) interacted preferentially with the base plate edge and rim. Similarly, a negatively charged complex of poly(allylamine hydrochloride) ('PAH') saturated with carbonate anions (ζ-potential of -2.8 ± 1 mV), remained bound to the base plate edge and rim (Fig. 4B). To confirm that the binding of the polymers was indeed to the rim, and to determine to which side (the "top" or "bottom"), we performed cryoET on base plates base plate stained with PAH saturated with carbonate ions. Indeed, the polymer remained bound to the top side only, confirming that this particular side provided a rather non-specific binding target for a range of negatively charged macromolecular complexes (Fig. 4C-D). Importantly, this is the same side of the base plate where crystal nucleation takes place and where Ca^{2+}-polysaccharide complexes bound to.

PAH or PAA alone, in the absence of carbonate or Ca^{2+} ions, respectively, do not provide enough contrast to be detected by cryoTEM (Cantaert et al., 2012). Therefore, cryo-TEM observations were complemented with super resolution 3D-Structured Illumination Microscopy ('3D-SIM') imaging, whereby PAA and PAH labelled with fluorescent dyes, Rhodamine 123 and fluorescein, respectively, were used to probe the base plate charge (Fig. S2) (Schermelleh et al., 2008). As expected, the negatively charged PAA was attracted to the biogenic material, resulting in base plates exhibiting fluorescence (Fig. 5A). Equipped with positively charged amine groups, PAH did not bind to the base plates dispersed in water. However,

when placed in an aqueous solution of sodium carbonate, the base plates attracted PAH, which correlated with the previously obtained cryoTEM data and confirmed that oversaturation of the polymer with carbonate ions and the consecutive neutralization of the positive charge triggered the polymer-base plate interaction. This transition was further evidenced by the observed change in the ζ-potential of the polymer measured in solutions containing different concentrations of carbonate ions (Fig. S3). It must be noted that while the resolution of 3D-SIM is *ca.* 150 nm, it is dependent on the sample, labelling intensity and fluorphore density (Cox, 2015). It is possible that the labelling conditions, in particular the tagging of the polymers with the fluorophores, still needs to be optimized to achieve a resolution high enough to resolve the dark internal area from the rim. Nevertheless, the fact that the polymers interacted preferentially with the base plate rim had been confirmed with nanometer resolution using cryoET.

Taking into account that any positive charge in a biological system was likely to originate from amine functionalities, the base plates were reacted with Alexa Fluor 488 activated with an N-hydroxysuccinimide ester ('NHS'). The functionalization of the Alexa Fluor with the NHS ester ensures a specific crosslinking reaction of the dye with primary amines, making this compound especially suited to label macromolecules that contain such functionality (Sueyoshi et al., 2011). The base plates were imaged with unprecedented spatial resolution of 60 nm using super-resolution radial fluctuations ('SRRF') microscopy (Gustafsson et al., 2016), which confirmed that the interaction of the dye was confined to the base plate edges (Fig. 5B), pointing to the presence of primary amines in those regions.

4. Discussion

Based on our data, we propose a model in which hydrated Pcar base plates display three levels of organization. The bottom side consists of highly symmetrical fibrils arranged in a lamellar pattern, whereby individual fibers aggregate to form the 'V'-shaped junctions between the neighboring lamellas. The middle part of the base plate contains well defined concentric fibers, whose existence was revealed before using shadow casting and negative staining experiments (Franke and Brown, 1971; Outka and Williams, 1971). The *ca.* 3 nm thin top part, which we report for the first time, is composed of a mesh-like fabric and displays a clearly different texture when imaged in the center of the base plate and at the rim, strongly indicating differences in its macromolecular components. High-resolution cryoET was fundamental to solve the structure of the base plate in 3D, confirming the presence of a complex tiered architecture that was proposed based on extrapolating from 2D TEM data on dry specimens. Additionally, we show that PAA and negatively charged complexes of PAH-CO_3^{2-}, both of which are devoid of secondary structure, bind to the rim of the base plates and deliver Ca^{2+} and CO_3^{2-} ions, respectively, to these regions. These observations, together with the Alexa Fluor labelling, suggests that the rim of the base plates, which contain crystal nucleation sites, are functionalized with positively charged primary amines (Figure 4C). The 3D structure and surface functionality of the base plates will be discussed below.

4.1 Three-dimensional structure of the base plate

Previous studies have identified that the base plates from Pcar contain two morphologically-distinct sides: one composed of radial fibers emerging from a central region, which constitutes the "bottom" side, and the second composed of circular, concentric fibers, considered the "top" side – where $CaCO_3$ crystals nucleate (Franke and Brown, 1971; Gal et al., 2016; Outka and Williams, 1971; Pienaar, 1969). These studies were conducted on dehydrated specimens, and employed imaging methods such as shadow-casting and negative staining in TEM, or atomic force microscopy, which is a surface technique. Therefore, it was not possible, based on these observations, to infer how these distinct structures are organized in 3D. Importantly, the dehydration caused by the sample preparation methods can cause artefacts such as shrinkage and the collapse of biological structure, effectively changing their morphology and organization.

Employing electron tomography on cryogenically-preserved specimens, we were able to characterize the structure of the base plates in 3D in their native, hydrated state. While we validated the presence of the two layers previously described, some differences were noted: (1) we identified, for the first time, the presence of a third layer composed of a thin meshwork of fibers, each 2-3 nm in diameter. This layer composes the top surface of the base plate (the side onto which crystal nucleation and growth takes

place), rather than the circular concentric fibers, as previously reported (Franke and Brown, 1971). The reason this layer was not visualized before is likely due to the lack in resolution of the previous imaging methods, shrinkage of the material after drying, and the superposition with the other layers of the base plate in 2D TEM imaging. (2) the circular concentric fibers that constitute the second layer of the base plates are *ca.* 3 nm wide, as opposed to 6-7 nm described by Franke and Brown (1971). We attribute these differences to the sample preparation method: Franke and Brown used negative staining to image the base plates, in which contrast is given by the *absence* of the staining agent. In other words, features in the specimen are visualized indirectly, due to their *lack* of heavy metal contrast. This likely resulted in the network of fibers appearing thicker in diameter. Additionally, the dehydration step involved in the sample preparation could also lead to the flattening of any cylindrical structures, making them seem wider than they actually are. (3) the rim of the base plate is 100 nm-wide and has a globular-like texture, not previously shown. Furthermore, these features cover the fibrous middle layer of the base plate. Given that the rim is the site where Ca^{2+}-polysaccharide complexes bind to, and such binding does not occur after treatment of the base plate with protease (Sakurada et al., 2018), we hypothesize that the structures observed here are composed of proteins and constitute the sites where calcium ions are delivered to. Cryo-electron tomography measurements on base plates treated with proteases need to be performed to confirm that.

4.2 Surface functionality of the base plate

The presence of positive charges on the rim of the base plates is consistent with the observation by Gal et al. (2016) that when mica surfaces functionalized with polylysine were used as substrates for AFM, the base plates always adsorbed with their mineral-associated side facing up. Such preferential absorption can only be explained by the electrostatic repulsion between the positively charged polylysine and the positive charges in the rim of the base plates. Indeed, we show that negatively charged PAA and a negatively charged complex of PAA-Ca^{2+} bind to the rim of the base plates while positively charged PAH only binds when saturated with carbonate ions, thus acquiring a negative net charge. Importantly, cryoET demonstrated that the binding occurs only on the 'top side' of the base plate, where crystal nucleation takes place. Considering that these polymers are simple polyelectrolytes with no secondary or tertiary structures (unlike proteins), their agglomeration on the surface of the base plate was most likely driven by electrostatic interactions between the negatively charged carboxylic acid moieties in PAA or the carbonates in the PAH-carbonate complex and positively charged donors attached to the top side of the rim, whose presence has not been reported before. Indeed, base plates stained with sodium phosphotungstate displayed a similar behavior, whereby phosphotungstate anions were attracted selectively to the base plate rim. Considering that neither PAA nor phosphotungstic acid have a known biological role, the observed binding had to be driven rather by electrostatic forces than by highly specific supramolecular interactions evolved to resemble a targeted key-hole type binding mechanism.

The staining with Alexa Fluor-NHS indicates that the positive charges derive from the presence of primary amine functionalities that are confined to the rim of the Pcar base plates. It must be noted, though, that the base plates appeared more elliptical than observed in our cryoTEM images. We attribute that to the fact that the samples were embedded in a low-background resin and were free to adopt any orientation in the three-dimensional space, in this case being tilted with respect to the focal plane of the microscope. Likewise, we attribute the stronger staining at the poles of the base plates to the superposition of their top circumference when tilted. We suggest that the primary amines derive from lysine side chains on proteins that are present on the rim of the base plates and are accessible to other species present within the mineralization vesicle, such as CAPs/Ca^{2+} complexes. This hypothesis is supported by recent data showing that CAP/Ca^{2+} complexes do not bind to base plates which had the protein component removed by proteases (Sakurada et al., 2018). Although we recognize that microscopy methods alone are insufficient to determine the exact structure of compounds present on the base plate surface, the presented approach enabled us to carry out a preliminary characterization of the base plate rim.

Considering that positively charged surfaces have been confirmed to discourage calcite formation on many occasions (Ravenhill et al., 2017; Wucher et al., 2007), we speculate that one of the roles of the

CAPs must involve transporting Ca^{2+} ions and directing them to the preferred calcite nucleation sites as neutral or negatively charged complexes. We propose that electrostatic interactions and hydrogen bonds occurring between the amine functionalities of the base plate rim and the carboxylic acid functionalities of CAPs are the dominant forces directing CAPs-Ca^{2+} complexes to the precise locations where calcite nucleation and growth take place (Gal et al., 2016; Gal et al., 2017a). Furthermore, considering that this Ca^{2+} ions transport strategy is necessary to induce calcite precipitation, our proposed model correlates with the previously observed phenomenon whereby the remineralization of coccolith base plates *in vitro* was achievable only if CAPs were also present as additives in the crystal growth mixture (Gal et al., 2017a). However, considering that CAPs were confirmed to interact with Pcar base plates only in the presence of Ca^{2+} ions (Gal et al., 2016), we propose that CAPs undergo a conformational change upon interacting with the latter, which enables them to bind to the base plates. Such a transition must be required to impart selectivity into the described mechanism, verifying that only these CAPs that transport Ca^{2+} ions can bind to the base plates, and that any excessive, Ca^{2+}-free molecules do not block any potential nucleation site. Overall, while it is possible that specific macromolecular recognition is responsible for the binding of the Ca^{2+}-CAPs complexes to the rim of the base plates, as proposed by Gat *et al*. (2016) our results demonstrate that non-specific electrostatic interactions are sufficient to mediate this process and may play a role in directing the binding of negatively charged CAPs to deliver Ca^{2+} ions specifically to the mineralization sites.

5. Conclusions

In conclusion, we show that the combination of CryoTEM, CryoET, and super-resolution optical microscopy can be used to probe the surface functionality of biogenic mineralization templates, such as coccolith base plates. Using Pcar as a model organism, we determined the structure of the base plates in their native, hydrated state, and discovered that it is composed of three distinct layers. We provide evidence that the rim of the base plates, where crystal nucleation takes place, is functionalized with positively charged primary amines, suggesting that electrostatic interactions play a role in mediating the interactions between the base plates, CAPs, and Ca^{2+} cations. Our future work will build on the presented preliminary characterization of Pcar base plates' surface and will aim to provide a greater understanding of the temporal evolution of coccoliths, establishing factors that direct their morphological development, and investigating the origin of alternating crystallographic orientations of neighboring calcite units.

References

Ackermann, H.-W., 2009. Basic Phage Electron Microscopy, p. 113-126, in: M. R. J. Clokie and A. M. Kropinski, Eds.), Bacteriophages: Methods and Protocols, Volume 1: Isolation, Characterization, and Interactions, Humana Press, Totowa, NJ.

Begum, G., Singh, S., Rangaraj, N., Srinivas, G., Rana, R.K., 2010. Cellular permeation with nuclear infiltration capability of biomimetically synthesised fluorescent monodisperse mesoporous silica nanospheres in HeLa and human stem cells. J. Mater. Chem. 20, 8563-8570.

Cantaert, B., Kim, Y.-Y., Ludwig, H., Nudelman, F., Sommerdijk, N.A.J.M., Meldrum, F.C., 2012. Think Positive: Phase Separation Enables a Positively Charged Additive to Induce Dramatic Changes in Calcium Carbonate Morphology. Adv. Funct. Mater. 22, 907-915.

Chu, C., Darling, K., Netusil, R., Doyle, R.P., Zubieta, J., 2011. Synthesis and structure of a lead(II)-citrate: {Na(H2O)(3)}[Pb-5(C6H5O7)(3)(C6H6O7)(H2O)(3)]center dot 9.5H(2)O. Inorg Chim Acta 378, 186-193.

Cox, S., 2015. Super-resolution imaging in live cells. Dev Biol 401, 175-181.

Crenshaw, M.A., Ristedt, H., 1976. The histochemical localization of reactive groups in septal nacre from Nautilus pompilius, p. 355-367, in: N. Watabe and K. M. Wilbur, Eds.), The Mechanisms of Mineralization in the Invertebrates and Plants, University of South Carolina Press, Colombia.

Drzewiecka-Antonik, A., Koziol, A.E., Rejmak, P., Lawniczak-Jablonska, K., Nittler, L., Lis, T., 2017. Novel Ba(II) and Pb(II) coordination polymers based on citric acid: Synthesis, crystal structure and DFT studies. Polyhedron 132, 1-11.

Franke, W.W., Brown, R.M., 1971. Scale Formation in Chrysophycean Algae .3. Negatively Stained Scales of Coccolithophorid Hymenomonas. Arch Mikrobiol 77, 12-&.

Gal, A., Wirth, R., Kopka, J., Fratzl, P., Faivre, D., Scheffel, A., 2016. Macromolecular recognition directs calcium ions to coccolith mineralization sites. Science 353, 590-593.

Gal, A., Wirth, R., Barkay, Z., Eliaz, N., Scheffel, A., Faivre, D., 2017a. Templated and self-limiting calcite formation directed by coccolith organic macromolecules. Chem. Commun. 53, 7740-7743.

Gal, A., Sorrentino, A., Kahil, K., Pereiro, E., Faivre, D., Scheffel, A., 2018. Native-state imaging of calcifying and noncalcifying microalgae reveals similarities in their calcium storage organelles. P Natl Acad Sci USA 115, 11000-11005.

Gal, A., Sviben, S., Wirth, R., Schreiber, A., Lassalle-Kaiser, B., Faivre, D., Scheffel, A., 2017b. Trace-Element Incorporation into Intracellular Pools Uncovers Calcium-Pathways in a Coccolithophore. Advanced Science 4.

Gustafsson, N., Culley, S., Pereira, P.M., Henriques, R., Gustafsson, N., Ashdown, G., Owen, D.M., 2016. Fast live-cell conventional fluorophore nanoscopy with ImageJ through super-resolution radial fluctuations. Nat. Commun. 7, 12471.

Henriksen, K., Stipp, S.L.S., Young, J.R., Marsh, M.E., 2004. Biological control on calcite crystallization: AFM investigation of coccolith polysaccharide function. American Mineralogist 89, 1709-1716.

Jackson, C.L., Chanzy, H.D., Booy, F.P., Drake, B.J., Tomalia, D.A., Bauer, B.J., Amis, E.J., 1998. Visualization of Dendrimer Molecules by Transmission Electron Microscopy (TEM): Staining Methods and Cryo-TEM of Vitrified Solutions. Macromolecules 31, 6259-6265.

Kayano, K., Saruwatari, K., Kogure, T., Shiraiwa, Y., 2011. Effect of coccolith polysaccharides isolated from the coccolithophorid, Emiliania huxleyi, on calcite crystal formation in in vitro CaCO3 crystallization. Mar Biotechnol (NY) 13, 83-92.

Kremer, J.R., Mastronarde, D.N., McIntosh, J.R., 1996. Computer visualization of three-dimensional image data using IMOD. J Struct Biol 116, 71-76.

Laguecir, A., Ulrich, S., Labille, J., Fatin-Rouge, N., Stoll, S., Buffle, J., 2006. Size and pH effect on electrical and conformational behavior of poly(acrylic acid): Simulation and experiment. Eur. Polym. J. 42, 1135-1144.

Lowenstam, H.A., Weiner, S., 1989. On Biomineralization Oxford University Press, New York.

Manton, I., Leedale, G.F., 1969. Observations on Microanatomy of Coccolithus Pelagicus and Cricosphaera Carterae with Special Reference to Origin and Nature of Coccoliths and Scales. Journal of the Marine Biological Association of the United Kingdom 49, 1-&.

Marsh, M.E., 1994. Polyanion-mediated mineralization-assembly and reorganization of acidic polysaccharides in the Golgi system of a coccolithophorid alga during mineral deposition. Protoplasma 177, 108-122.

Marsh, M.E., 1999. Coccolith crystals of *Pleurochrysis carterae*: crystallographic faces, organization, and development. Protoplasma 207, 54-66.

Nudelman, F., Gotliv, B.A., Addadi, L., Weiner, S., 2006. Mollusk shell formation: Mapping the distribution of organic matrix components underlying a single aragonitic tablet in nacre. Journal of Structural Biology 153, 176-187.

Outka, D.E., Williams, D.C., 1971. Sequential Coccolith Morphogenesis in Hymenomonas-Carterae. Journal of Protozoology 18, 285-&.

Pienaar, R.N., 1969. The fine structure of *Criscosphaera carterae*. Journal of Cell Science 4, 561-567.

Ravenhill, E.R., Adobes-Vidal, M., Unwin, P.R., 2017. Calcium carbonate crystallisation at charged graphite surfaces. Chem. Commun. 53, 12552-12555.

Sakurada, S., Fujiwara, S., Suzuki, M., Kogure, T., Uchida, T., Umemura, T., Tsuzuki, M., 2018. Involvement of Acidic Polysaccharide Ph-PS-2 and Protein in Initiation of Coccolith Mineralization, as Demonstrated by In Vitro Calcification on the Base Plate. Mar Biotechnol 20, 304-312.

Schermelleh, L., Carlton, P.M., Haase, S., Shao, L., Winoto, L., Kner, P., Burke, B., Cardoso, M.C., Agard, D.A., Gustafsson, M.G.L., Leonhardt, H., Sedat, J.W., 2008. Subdiffraction multicolor imaging of the nuclear periphery with 3D structured illumination microscopy. Science 320, 1332-1336.

Sueyoshi, K., Hashiba, K., Kawai, T., Kitagawa, F., Otsuka, K., 2011. Hydrophobic labeling of amino acids: Transient trapping-capillary/microchip electrophoresis. Electrophoresis 32, 1233-1240.

Sviben, S., Gal, A., Hood, M.A., Bertinetti, L., Politi, Y., Bennet, M., Krishnamoorthy, P., Schertel, A., Wirth, R., Sorrentino, A., Pereiro, E., Faivre, D., Scheffel, A., 2016. A vacuole-like compartment concentrates a disordered calcium phase in a key coccolithophorid alga. Nat. Commun. 7, 11228.

Taylor, A.R., Brownlee, C., Wheeler, G., 2017. Coccolithophore Cell Biology: Chalking Up Progress. Annual Review of Marine Sciences, Vol 9 9, 283-310.

van der Wal, P., de Jong, E.W., Westbroek, P., de Bruijn, W.C., Mulder-Stapel, A.A., 1983. Ultrastructural polysaccharide localization in calcifying and naked cells of the coccolithophoridEmiliania huxleyi. Protoplasma 118, 157-168.

Walker, J.M., Marzec, B., Lee, R.B.Y., Vodrazkova, K., Day, S.J., Tang, C.C., Rickaby, R.E.M., Nudelman, F., 2019. Polymorph Selectivity of Coccolith-Associated Polysaccharides from Gephyrocapsa Oceanica on Calcium Carbonate Formation In Vitro. Adv Funct Mater 29.

Wilbur, K.M., Watabe, N., 1963. Experimental studies on calcification in molluscs and the alga coccolithus huxleyi. Annals of the New York Academy of Sciences 109, 82-112.

Wucher, B., Yue, W., Kulak, A.N., Meldrum, F.C., 2007. Designer Crystals: Single Crystals with Complex Morphologies. Chem. Mater. 19, 1111-1119.

Young, J.R., Davis, S.A., Bown, P.R., Mann, S., 1999. Coccolith ultrastructure and biomineralisation. Journal of Structural Biology 126, 195-215.

Young, J.R., Didymus, J.M., Bown, P.R., Prins, B., Mann, S., 1992. Crystal Assembly and Phylogenetic Evolution in Heterococcoliths. Nature 356, 516-518.
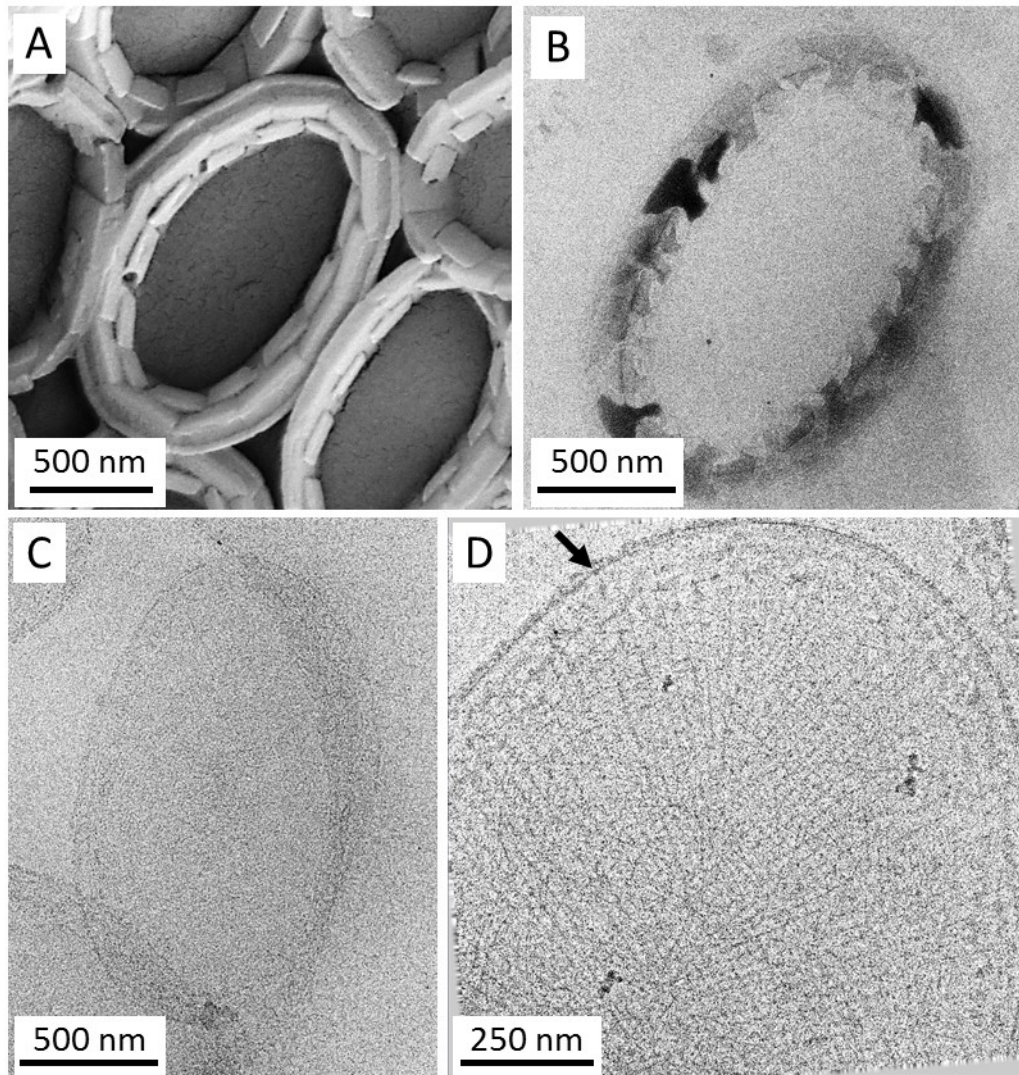
Figure 1. Base plates produced by *Pleurochrysis carterae*. (A) SEM image of Pcar coccoliths. **(B)** CryoTEM image of a Pcar coccolith prior to decalcification. **(C)** CryoTEM image of a decalcified base plate from Pcar. **(D)** High magnification cryoTEM image of a decalcified Pcar baseplate, revealing its fibrous structure. Black arrow: 10 nm-thick border of the base plate.
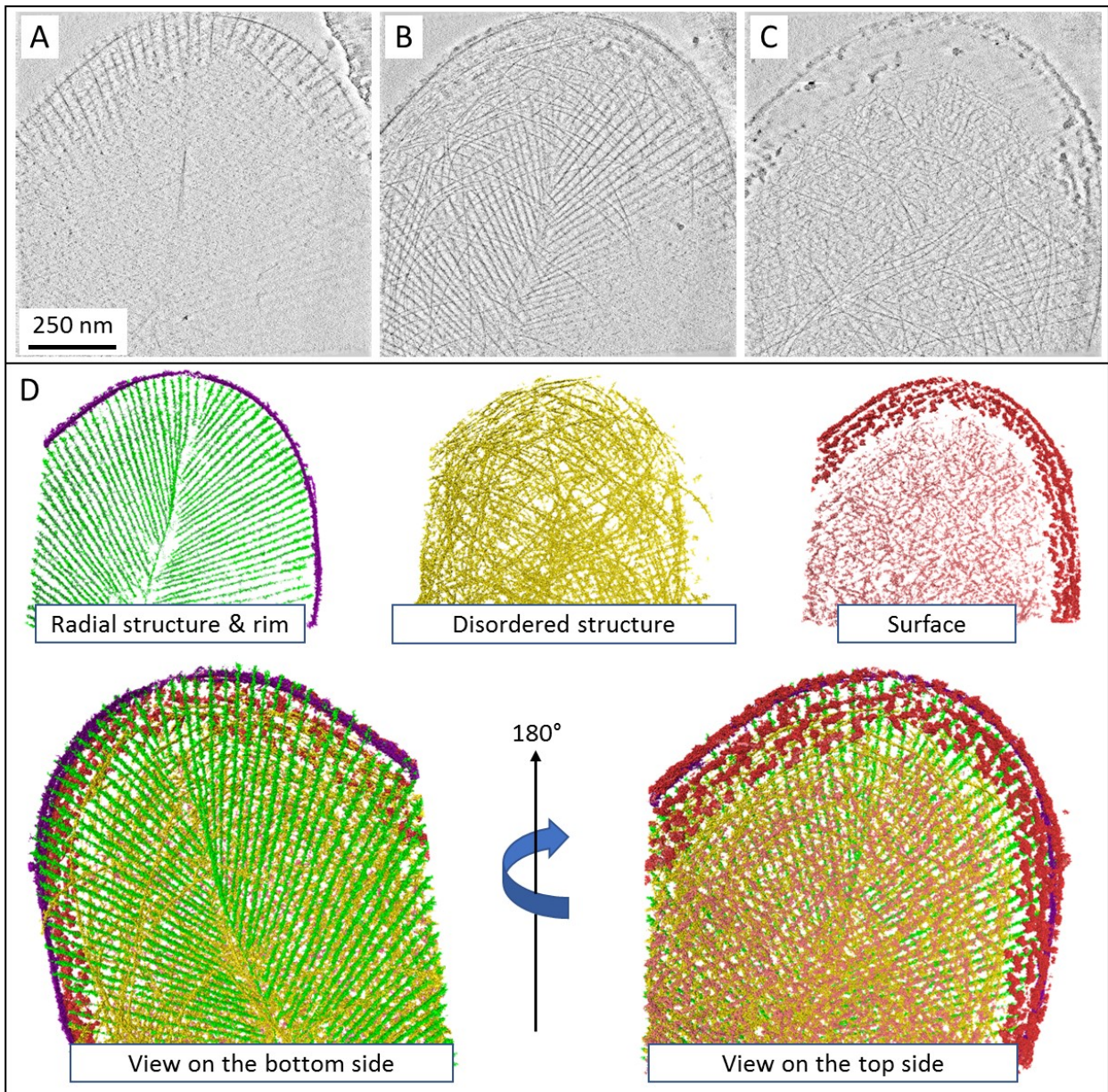
Figure 2. Cryo-electron tomography of a decalcified base plate from Pcar. (A-C) Exemplary *z*-slices from the tomographic reconstruction. **(D)** Segmentation of the obtained tomogram reveals the 3D structure of Pcar base plates in their native, hydrated state. *Color code:* green: radial structure at the bottom layer; violet: outer rim; yellow: circular fibers in the middle layer; red: top layer composed of a fine fibrous meshwork and globular-textured rim.
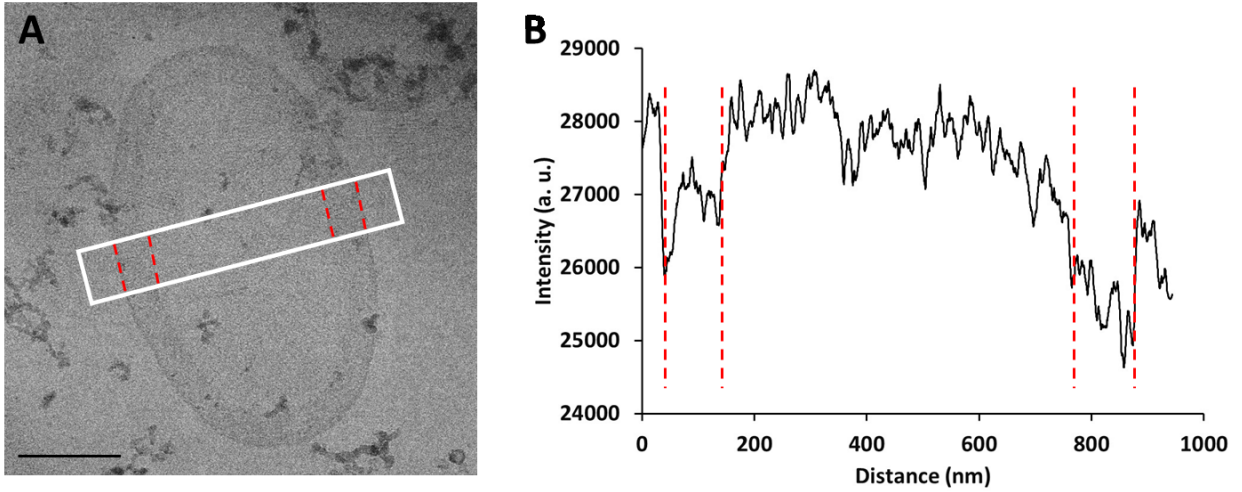
Figure 3. CryoTEM images of stained Pcar base plates. (A) CryoTEM image of a base plate stained with sodium phosphotungstate. The white box shows the area from where an intensity profile was taken, shown in **(B)**. The rim of the base plate, marked by the red dotted lines in **(A)** and **(B)**, has higher electron density than the middle of the base plate, as shown in the intensity profile in **(B)**. Scale bar: 500 nm.
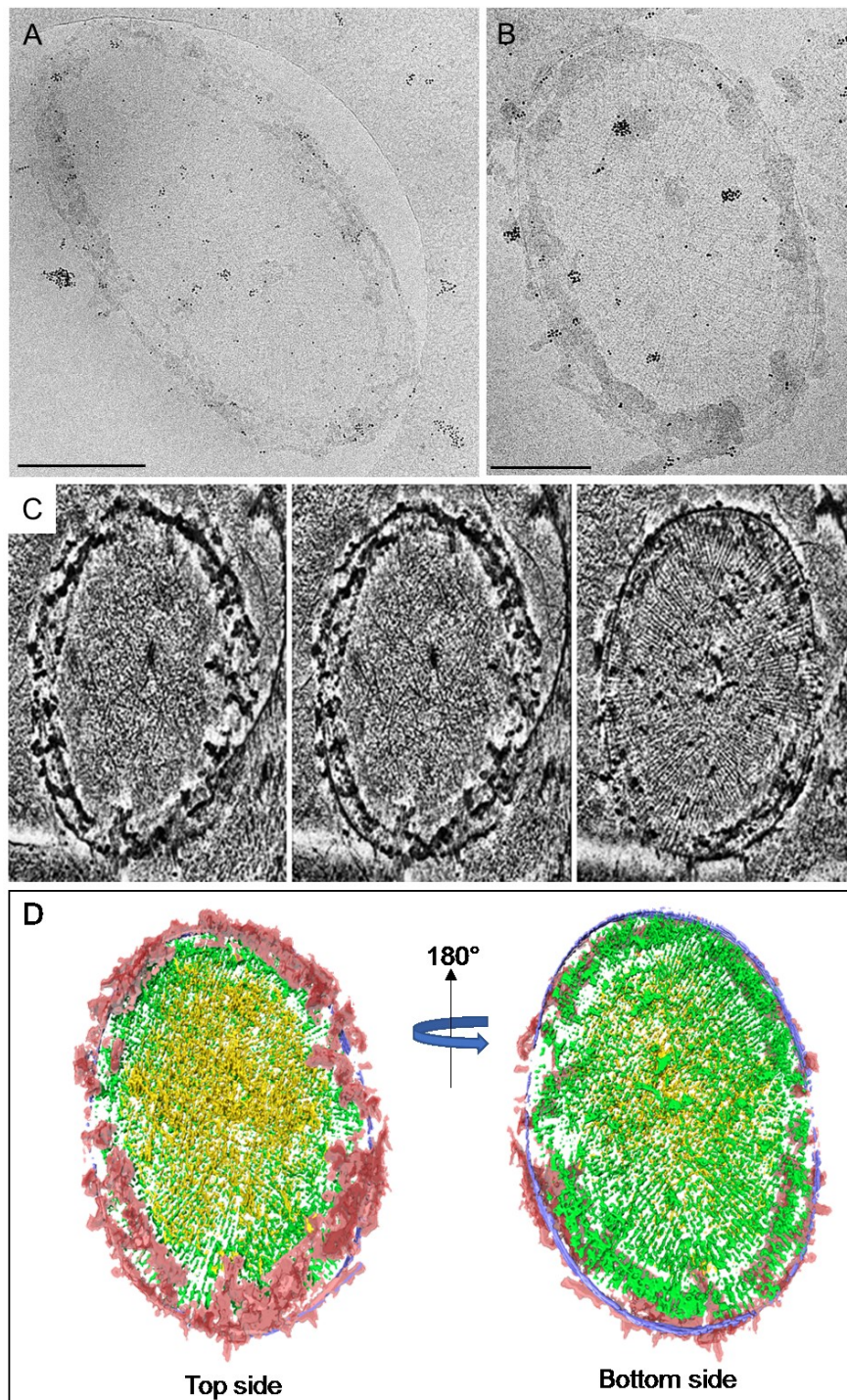
Figure 4. CryoTEM images of Pcar base plates treated with negatively and positively charged polymers. (A) Binding of a mixture of poly(acrylic acid) and Ca^{2+} ions to the base plate rim. **(B)** Binding of the mixture of poly(allylamine hydrochloride) ('PAH') saturated with carbonate anions to the base plate rim. **(C)** Three different *z*-slices from the tomographic reconstruction a Pcar base plate in the presence of PAH saturated with carbonate anions. **(D)** Segmentation of the cryoET experiment shown in **(C)** confirming that the mixture of PAH and CO_3^{2-} anions interacts preferentially with the top side of the base plate. *Scale bars:* 500 nm.
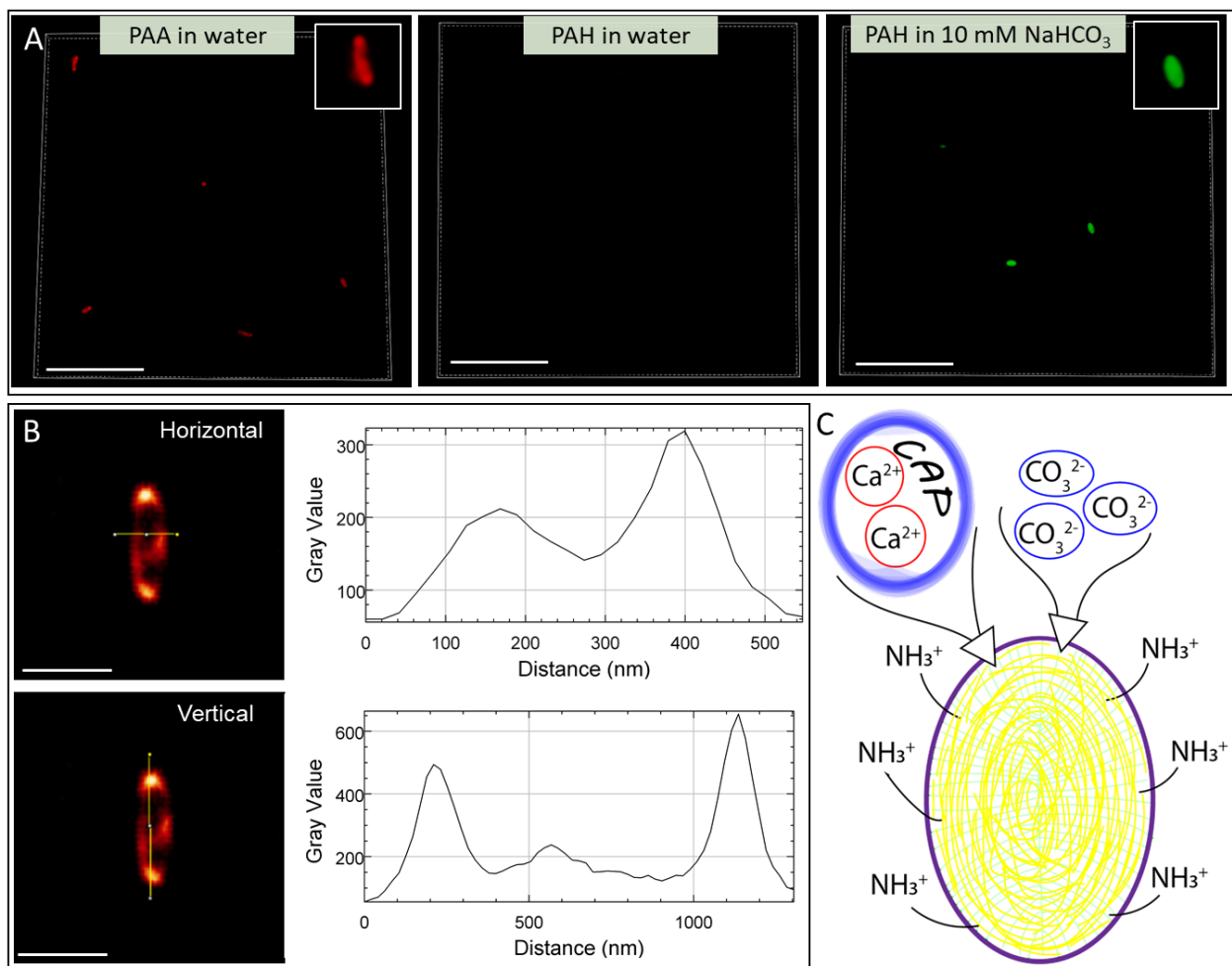
Figure 5. Stained Pcar base plates visualized using optical microscopy. (A) Structured Illumination Microscopy ('SIM') images of Pcar base plates stained with fluorescent probes: poly(acrylic acid) ('PAA') and poly(allylamine hydrochloride) ('PAH') dispersed in either water or 10 mM Na_2CO_3 confirm the electrostatic nature of polymer – base plate interactions. *Insets:* magnifications on exemplary base plates. *Scale bars:* 10 μm. **(B)** Super-Resolution Radial Fluctuations ('SRRF') microscopy image of base plates labelled with Alexa Fluor 488 NHS ester show the location of amine functionalities. The corresponding intensity profiles reveal the separation distances in the horizontal and vertical direction, respectively. *Scale bars:* 1 μm. **(C)** A model of the CAP – base plate interaction: positively charged amine groups are confined to the rim of the base plate top side and attract the negatively charged Ca^{2+}-CAP complexes and carbonate anions to that particular area, promoting localized nucleation and development of calcite single crystals.